Robust Plasmonic Hot-Spots in A Metamaterial Lattice for Enhanced Sensitivity of Infrared Molecular Detection

Atsushi Ishikawa,[1,2,3,4,a),†] Shuhei Hara,[1,†] Takuo Tanaka,[3,4,5] Xiang Zhang,[2,6,7,b)] and Kenji Tsuruta[1]

[1]*Department of Electrical and Electronic Engineering, Okayama University, Okayama, Okayama 700-8530, Japan.*

[2]*NSF Nanoscale Science and Engineering Center, University of California, Berkeley, CA 94720, USA.*

[3]*Metamaterials Laboratory, RIKEN, Wako, Saitama 351-0198, Japan.*

[4]*Innovative Photon Manipulation Research Team, RIKEN Center for Advanced Photonics, Wako, Saitama 351-0198, Japan.*

[5]*Department of Chemical Science and Engineering, Tokyo Institute of Technology, Yokohama, Kanagawa 226-8503, Japan.*

[6]*Materials Sciences Division, Lawrence Berkeley National Laboratory, Berkeley, CA 94720, USA.*

[7]*Department of Physics, King Abdulaziz University, Jeddah 21589, Saudi Arabia.*

[a)]Electronic mail: a-ishikawa@okayama-u.ac.jp.

[b)]Electronic mail: xiang@berkeley.edu.

[†]A.I and S.H. contributed equally to this work.

ABSTRACT

High-density and long-lived plasmonic hot-spots are an ideal system for high-sensitive surface-enhanced infrared absorption (SEIRA), but these conditions are usually incompatible due to unwanted near-field coupling between the adjacent unit structures. Here, by fully controlling plasmonic interference in a metamaterial lattice, we experimentally demonstrate densely-packed long-lived quadrupole plasmons for high-sensitive SEIRA. The metamaterial consists of a strongly-coupled array of super- and sub-radiant plasmonic elements to exhibit an electromagnetic transparency mode at 1730 cm^{-1}, which spectrally overlaps with the C=O vibrational mode. In the SEIRA measurement, the C=O mode of poly(methyl methacrylate) molecules is clearly observed as a distinct dip within a transmission peak of the metamaterial. The corresponding numerical simulations reveal that constructive interference uniformly forms coherent quadrupole plasmons over the metamaterial lattice, leading to a stronger molecular signal from the system. Our metamaterial approach provides a robust way to construct ideal hot-spots over the sample, paving the way toward a reliable sensing platform of advanced IR inspection technologies.

MAIN TEXT

Controlling the near-filed coupling of metallic nanostructures has played a central

role in the field of plasmonics with potential applications in integrated optics, solar energy

harvesting, and bio-chemical sensing.[1-4] Recent advances in nanofabrication have further

developed plasmonic complexes, allowing for interesting hybridized responses inaccessible

by individual elements.[5-8] In particular, it is well known that a plasmon mode can be either

super- or sub-radiant depending on radiative losses, and their coupling gives rise to

asymmetric Fano resonance with the steep dispersion.[9-11] The quality factor of Fano

resonance can be also very high by engineering their coupling strengths, thereby efficiently

trapping the incident light into a long-lived sub-radiant mode.[12,13] Such

geometry-dependent plasmon characteristics offer a new capability to manipulate optical

confinement at the nanoscale, i.e., plasmonic hot-spots, as well as their spectral

responses.[14,15] A plasmonic metamaterial is an advanced example,[16-18] where macroscopic

optical properties, permittivity and permeability, of plasmonic ensembles can be tailored at

will, overcoming fundamental limitations in conventional optics.[19-25]

Surface-enhanced infrared absorption (SEIRA) is the promising application by fully utilizing plasmonic resonant nature for strong optical interaction with molecules.[26] Plasmonic hot-spots have been traditionally investigated on metal island films, but they suffer from poor reproducibility due to the uncontrolled surface nanostructures.[27] Well-defined plasmons in optical nanoantennas were recently proposed for the resonant SEIRA where the spatial and spectral mode overlapping were dramatically improved between the plasmons and molecular vibrations.[28-33] Engineered IR metamaterials were also demonstrated for the background-suppressed SEIRA to gain a large vibrational signal contrast for better sensitivity.[34,35] Based on such hot-spot engineering in tailored plasmonic nanostructures, atto/zeptomole sensitivity of SEIRA is now practically possible for specific conditions. On the other hand, for reliable IR inspection of small amounts of molecules, the surface density of hot-spots over the sample is also crucial to trap as many as possible of molecules contributing to the vibrational signal from the system.[36] However, once plasmonic elements with enhanced hot-spots are closely packed, unwanted near-field coupling between the adjacent unit structures usually modifies their mode profiles, thereby

rendering the hot-spots broad and weak; therefore, increasing the hot-spots density while maintaining their quality factors remains a major challenge.[37-40]

Here, we address this issue by fully controlling plasmonic interference in a metamaterial lattice for high-sensitive SEIRA. Specifically, we study the near-field coupling in a metamaterial consisting of a strongly-coupled array of super- and sub-radiant plasmonic elements to exhibit classical analogue of electromagnetically induced transparency (EIT) arising from Fano resonance.[41-44] Different from our previous work,[35] we introduce lateral displacement of the unit cells in the EIT metamaterial to engineer their near-filed coupling and the resultant spectral response. Based on constructive interference of long-lived quadrupole plasmons in the lattice, highly-dispersive dense hot-spots are uniformly formed over the sample. The high-sensitive SEIRA is then demonstrated by utilizing the resonant coupling between the EIT mode of the metamaterial and IR vibrational mode of polymer molecules.

Figure 1(a) shows the schematic super-cell of the fabricated EIT metamaterial consisting of four unit cells where each unit cell is made of a horizontal Au bar coupled

with a pair of vertical Au bars. The overall structure of the metamaterial was carefully

designed by considering not only the intra-/inter-unit cell coupling, but also their balance.

The fabrication process started with spin-coating of a 100-nm thick poly(methyl

methacrylate) (PMMA) resist (MicroChem, 950-A2) onto a 325-µm thick double-side

polished non-dope Si substrate. A two-dimensional periodic pattern of the metamaterial was

exposed by an electron beam (EB) lithography system (Elionix, ELS-S50) over an area of

100×100 µm^2. The sample was then completed by Cr/Au (2/20 nm) deposition using a

resistive heating evaporator and liftoff process. The geometrical parameters were: $w = 200$,

$l_{x(y)} = 950$ (850), $g_{x(y)} = 550$ (150), and $P_{x(y)} = 1500$ (1350) nm, respectively. As shown in

the scanning electron microscopy (SEM) images [Figs. 1(b)-(d)], three types of the

metamaterials were fabricated with different lateral displacements of $d = 0$ (green), $P_x/4$

(blue), and $P_x/2$ (red) to control the near-filed coupling among the adjacent unit cells.

Depending on plasmonic interference in the lattice, the quadrupole mode in the bar pairs is

constructively excited at 1730 cm^{-1}, which spectrally overlaps with the C=O vibrational

mode.

The transmission properties of the metamaterials were experimentally characterized

by using a Fourier-Transform Infrared Spectrometer (FT-IR) equipped with a polarized

infrared microscope (JASCO, FT/IR-6300FV and VIRT-3000). To improve the

signal-to-noise ratio of the spectra, a square aperture with an area of 100×100 μm^2 was

installed at the pupil plane of the microscope and a sample chamber was purged with dry

nitrogen gas. Figure 2(a) shows the measured transmission spectra of the metamaterials with

different lateral displacements for the x-polarized incident light. Here, the measured spectra

were normalized by that of a bare Si substrate to discuss only the optical responses of the

metamaterials. Without a lateral displacement of $d = 0$ (green), a typical transmission dip is

observed in the shaded region due to the dipole plasmon resonance of the horizontal bars.

For $d = P_x/4$ (blue) and $P_x/2$ (red), on the other hand, an EIT-like transmission peak clearly

appears within the dip due to constructive interference of the quadrupole plasmons in the

lattice. These observations are well supported by the corresponding numerical results in Fig.

2(b), which were obtained by using the three-dimensional electromagnetic simulation

software, CST Microwave Studio, with $\varepsilon_{Si} = 11.56$ and the empirical value for ε_{Au}.[45] For the

y-polarization, on the other hand, only the dipole plasmon resonance of the vertical bars was observed at a higher frequency (see supplementary material Fig. S1).

Figure 3 shows the corresponding mode profiles of the metamaterials at 1750 cm^{-1} in Fig. 2(b). Note that Figs. 3(b) and 3(c) are plotted using the same color bar such that the amplitude of J_x and J_y can be directly compared each other. In the unit cell level, the x-polarized incident light is predominantly coupled to the dipole mode in the horizontal bars, and then the quadrupole mode in the bar pairs is excited through the near-field coupling. The plasmonic interference between these super- and sub-radiant (dipole and quadrupole) modes forms Fano resonance characterized by an EIT-like optical response. In the metamaterial lattice, however, the additional near-filed coupling among the adjacent unit cells dramatically modifies the mode profiles and resultant spectral responses. In the case of $d = 0$ (the left column), since the charge distributions of the quadrupole mode in the bar pairs always conflict between the vertical neighboring unit cells, the quadrupole mode is strictly prohibited; therefore, only the dipole mode in the horizontal bars is allowed in the lattice, exhibiting to a single transmission dip, as shown in Fig. 2. For $d = P_x/2$ (the right

column), on the other hand, a half-period lateral displacement allows constructive interference of the quadrupole plasmons through the horizontal bars within the super-cell. Such a mode profile coherently extends over the lattice to exhibit a pronounced EIT-like transmission peak, as shown in Fig. 2. The $d = P_x/4$ (the center column) case is the intermediate state where both the dipole and quadrupole modes are excited simultaneously.

Since the metamaterial lattice with $d = P_x/2$ offers not only a highly-dispersive EIT spectral response but also high-density hot-spots over the sample, it can be a robust and reliable sensing platform for high-sensitive SEIRA. Here, we explore EIT metamaterial-enhanced IR absorption by utilizing the resonant coupling between the plasmonic modes of the metamaterials and IR vibrational modes of molecules. In the SEIRA measurement, PMMA was used as a test specimen to exhibit a typical C=O stretching vibrational mode at 1730 cm^{-1}. PMMA resist (MicroChem, 950-A2) was uniformly spin-coated onto the bare metamaterial surface with a thickness of 50 nm, which was determined by using an optical surface profiler (Zygo, NewView 7300). Using the PMMA molecular weight (950×10^3) and solid density (1.2 g/cm^3), ~630-attomole PMMA

molecules, i.e., $\sim 3.6 \times 10^{12}$ C=O bonds, existed within the sample area (100×100 μm^2) for the current experimental condition. Figure 4(a) shows the measured transmission spectra of the PMMA-coated metamaterials with different lateral displacements. Minor absorption dips near 1450 cm^{-1} and 1380 cm^{-1} are due to CH$_2$ and CH$_3$ bending vibrational modes. In the case of $d = 0$ (green), the resonant coupling between the dipole and C=O modes produces a clear anti-resonant peak within a transmission dip of the metamaterial. For $d = P_x/2$ (red), on the other hand, a distinct anti-resonant dip appears within an EIT-like transmission peak of the metamaterial. The molecular signal strength for the $d = P_x/2$ (red) case is about 2 times larger than that of the $d = 0$ (green) case; this can be naturally understood by considering the double hot-spots density in the $d = P_x/2$ (red) lattice, compared to that of the $d = 0$ (green) lattice. Note that such enhanced sensitivity was also obtained for the unpolarized incident light (see supplementary material Fig. S2).

To better understand the underlying mode interactions in the metamaterial-molecular coupled system, another set of numerical simulations was carried out as shown in Fig. 4(b). In the calculation, the C=O bond in the PMMA layer was

10

modeled as a Lorentz oscillator with the functional form: $\varepsilon_{PMMA} = \varepsilon_b + \frac{f_m \omega_0^2}{\omega_0^2 - \omega^2 - i\gamma\omega}$, where

ε_b is the background relative permittivity, f_m is the reduced oscillator strength, ω_0 is the

C=O vibrational frequency, and γ is the damping constant (FWHM).[33,46] The parameters, ε_b,

f_m, ω_0, and γ, were appropriately chosen such that the oscillator model emulated the

vibrational absorption of the C=O mode. An excellent agreement between the experiment

and simulation was obtained not only for the signal strength but also for deformation of the

spectral line-shape of each metamaterial lattice.

Fig. 4(c) shows the corresponding |E| distributions at $\omega_{C=O}$ in Fig. 4(b). In the

metamaterial-molecular coupled system, the C=O mode behaves as a local oscillator with a

finite absorption to disturb each metamaterial lattice in different ways. In the case of $d = 0$

(the left), the C=O mode quenches the dipole plasmons in the horizontal bars, producing a

typical anti-resonant peak within a transmission dip of the metamaterial. Compared to the

left (green) of Fig. 3(d), the mode profile in the horizontal bars remains the same, but the

electric field intensity around the bars drops by ~ 70% due to the quenching by the C=O

mode. For $d = P_x/2$ (the right), on the other hand, the C=O mode strongly disturbs sensitive

interference of the quadrupole plasmons in the lattice, rather than the quenching. As a result,

the pure quadrupole mode [the right (red) of Fig. 3(d)] is dramatically modified as a

mixture of the dipole and quadrupole modes, translating into distinct far-field spectral

responses. Such a highly-dispersive dense quadrupole mode contributes to a stronger

molecular signal compared to the dipole mode case for $d = 0$ (the left). Note that additional

evaluation in the SEIRA measurement (see supplementary material Fig. S3) showed the

ultimate sensing capability of the metamaterial lattice was zeptomole level, which is

comparable to the previous works.[33,35]

In conclusion, a spectroscopic technique based on high-density and long-lived

hot-spots was proposed and demonstrated by fully controlling plasmonic interference in an

EIT metamaterial lattice. The resonant coupling of the EIT mode of the metamaterial and

IR vibrational mode of polymer molecules was demonstrated for high-sensitive SEIRA.

The corresponding numerical simulations revealed that constructive interference uniformly

forms coherent quadrupole plasmons over the metamaterial lattice, leading to a stronger

molecular signal from the system. Our approach based on robust hot-spots in a

metamaterial lattice may hold great promise for realizing a reliable sensing platform of advanced IR inspection technologies.

See supplementary material for the polarization dependence of the transmission spectra and the ultimate sensing capability of the metamaterial lattice.

REFERENCES

[1] S. Lal, S. Link, and N. J. Halas, Nat. Photon. **1**, 641 (2007).

[2] J. A. Schuller, E. S. Barnard, W. Cai, Y. C. Jun, J. S. White, and M. L. Brongersma, Nat. Mater. **9**, 193 (2010).

[3] H. A. Atwater and A. Polman, Nat. Mater. **9**, 205 (2010).

[4] M. L. Brongersma, N. J. Halas, and P. Nordlander, Nat. Nanotech. **10**, 25 (2015).

[5] E. Prodan, C. Radloff, N. J. Halas, and P. Nordlander, Science **302**, 419 (2003).

[6] N. Liu, H. Guo, L. Fu, S. Kaiser, H. Schweizer, and H. Giessen, Adv. Mater. **19**, 3628 (2007).

[7] N. Tate, H. Sugiyama, M. Naruse, W. Nomura, T. Yatsui, T. Kawazoe, and M. Ohtsu, Opt. Express **17**, 11113 (2009).

[8] M. Hentschel, M. Saliba, R. Vogelgesang, H. Giessen, A. P. Alivisatos, and N. Liu, Nano Lett. **10**, 2721 (2010).

[9] U. Fano, Phys. Rev. **124**, 1866 (1961).

[10] A. E. Miroshnichenko, S. Flach, and Y. S. Kivshar, Rev. Mod. Phys. **82**, 2257 (2010).

[11] B. lukyanchuk, N. I. Zheludev, S. A. Maier, N. J. Halas, P. Nordlander, H. Giessen, and C. T. Chong, Nat. Mater. **9**, 707 (2010).

[12] A. Christ, Y. Ekinci, H. H. Solak, N. A. Gippius, S. G. Tikhodeev, and O. J. F. Martin, Phys. Rev. B **76**, 201405(R) (2007).

[13] F. Hao, P. Nordlander, Y. Sonnefraud, P. V. Dorpe, and S. A. Maier, ACS Nano **3**, 643 (2009).

[14] A. Moreau, C. Ciraci, J. J. Mock, R. T. Hill, Q. Wang, B. J. Wiley, A. Chilkoti, and D. R. Smith, Nature **492**, 86 (2012).

[15] T. Søndergaard, S. M. Novikov, T. Holmgaard, R. L. Eriksen, J. Beermann, Z. Han, K. Pedersen, and S. I. Bozhevolnyi, Nat. Commun. **3**, 969 (2012).

[16] C. M. Soukoulis, S. Linden, and M. Wegener, Science **315**, 47 (2007).

[17] N. I. Zheludev and Y. S. Kivshar, Nat. Mater. **11**, 917 (2012).

[18] N. Meinzer, W. L. Barnes, and I. R. Hooper, Nat. Photon. **8**, 889 (2014).

[19] W. Cai, U. K. Chettiar, A. V. Kildishev, and V. M. Shalaev, Nat. Photon. **1**, 224 (2007).

[20] M. Choi, S. H. Lee, Y. Kim, S. B. Kang, J. Shin, M. H. Kwak, K.-Y. Kang, Y.-H. Lee, N. Park, and B. Min, Nature **470**, 369 (2011).

[21] P. Moitra, Y. Yang, Z. Anderson, I. I. Kravchenko, D. P. Briggs, and J. Valentine, Nat. Photon. **7**, 791 (2013).

[22] R. Maas, J. Parsons, N. Engheta, and A. Polman, Nat. Photon. **7**, 907 (2013).

[23] H. Suchowski, K. O'Brien, Z. J. Wong, A. Salandrino, X. Yin, and X. Zhang, Science, **342**, 1223 (2013).

[24] A. M. Mahmoud and N. Engheta, Nat. Commun. **5**, 5638 (2014).

[25] B. Shen, R. Polson, and R. Menon, Adv. Nat. Commun. **7**, 13126 (2016).

[26] M. Osawa and M. Ikeda, J. Phys. Chem. **95**, 9914 (1991).

[27] T. R. Jensen, R. P. Van Duyne, S. A. Johnson, and V. A. Maroni, Appl. Spec. **54**, 371 (2000).

[28] F. Neubrech, A. Pucci, T. W. Cornelius, S. Karim, A. Garcia-Etxarri, and J. Aizpurua, Phys. Rev. Lett. **101**, 157403 (2008).

[29] R. Adato, A. A. Yanik, J. J. Amsden, D. L. Kaplan, F. G. Omenetto, M. K. Hong, S. Erramilli, and H. Altug, PNAS **109**, 19227 (2009).

[30] E. Hendry, T. Carpy, J. Johnston, M. Popland, R. V. Mikhaylovskiy, A. J. Lapthorn, S. M. Kelly, L. D. Barron, N. Gadegaard, and M. Kadodwala, Nat. Mater. **5**, 783 (2010).

[31] C. Wu, A. B. Khanikaev, R. Adato, N. Arju, A. A. Yanik, H. Altug, and G. Shvets, Nat. Mater. **11**, 69 (2012).

[32] L. V. Brown, K. Zhao, N. King, H. Sobhani, P. Nordlander, and N. J. Halas, J. Am. Chem. Soc. **135**, 3688 (2013).

[33] F. Cheng, X. Yang, and J. Gao, Sci. Rep. **5**, 14327 (2015).

[34] A. Ishikawa and T. Tanaka, Sci. Rep. **5**, 12570 (2015).

[35] A. Ishikawa, S. Hara, T. Tanaka, Y. Hayashi, and K. Tsuruta, Sci. Rep. **7**, 3205 (2017).

[36] X.-M. Li, M.-H. Bi, L. Cui, Y.-Z. Zhou, X.-W. Du, S.-Z. Qiao, and J. Yand, Adv. Func. Mater. **27**, 1605703 (2017).

[37] V. A. Fedotov, N. Papasimakis, E. Plum, A. Bitzer, M. Walther, P. Kuo, D. P. Tsai, and N. I. Zheludev, Phys. Rev. Lett. **104**, 223901 (2010).

[38] C. Yan and O. J. F. Martin, ACS Nano **8**, 11860 (2014).

[39] Y. Moritake, Y. Kanamori, and K. Hane, Appl. Phys. Lett. **107**, 211108 (2015).

[40] M. Wenclawiak, K. Unterrainer, and J. Darmo, Appl. Phys. Lett. **110**, 261101 (2017).

[41] C. L. G. Alzar, M. A. G. Martinez, and P. Nussenzveig, Am. J. Phys. **70**, 37 (2002).

[42] S. Zhang, D. A. Genov, Y. Wang, M. Liu, and X. Zhang, Phys. Rev. Lett. **101**, 047401 (2008).

[43] N. Verellen, Y. Sonnefraud, H. Sobhani, F. Hao, V. V. Moshchalkov, P. V. Dorpe, P. Nordlander, and S. A. Maier, Nano Lett. **9**, 1663 (2009).

[44] N. Liu, L. Langguth, T. Weiss, J. Kastel, M. Fleischhauer, T. Pfau, and H. Giessen, Nat. Mater. **8**, 758, (2009).

[45] P. B. Johnson and R. W. Christy, Phys. Rev. B **6**, 4370 (1972).

[46] J. D. Jackson, *Classical Electrodynamics* (John Wiley & Sons, Inc, 1999).
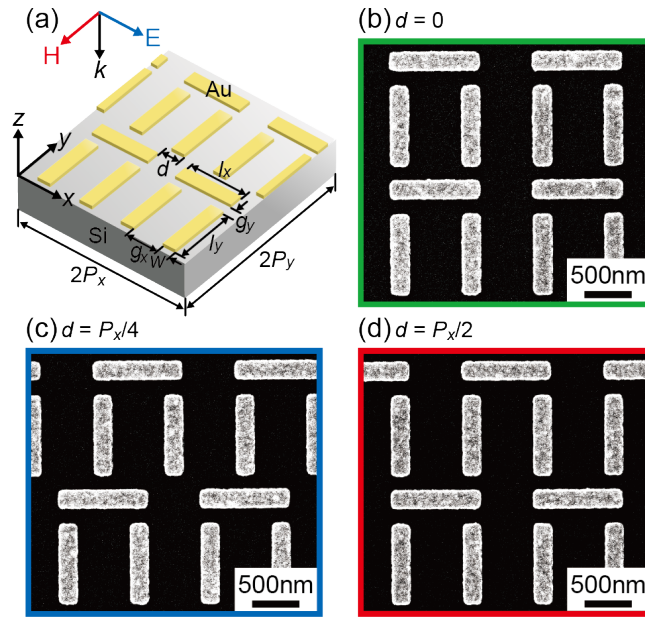
FIGURES

FIG 1. Design and fabrication of metamaterials. (a) Schematic super-cell of an EIT metamaterial on a Si substrate consisting of 20-nm thick Au bars coupled with Au bar pairs. The geometrical parameters are: w = 200, $l_{x(y)}$ = 950 (850), $g_{x(y)}$ = 550 (150), and $P_{x(y)}$ = 1500 (1350) nm, respectively. (b)-(d) SEM images of the fabricated metamaterials with different lateral displacements of d = 0 (green), $P_x/4$ (blue), and $P_x/2$ (red) to control the near-field coupling among the adjacent unit cells, thereby tuning the excitation of the EIT mode at 1730 cm^{-1}.
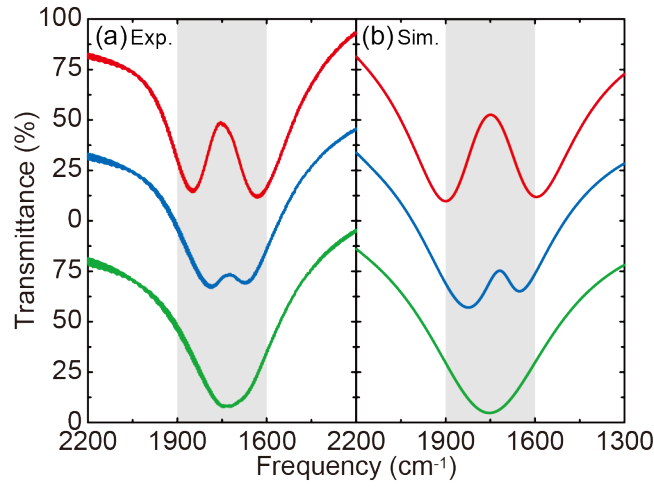
FIG 2. IR characterization of metamaterials. (a) Experimentally measured transmission spectra of the metamaterials and (b) corresponding numerical results, which well reproduced the experimental ones qualitatively and quantitatively. With a lateral displacement, an EIT-like transmission peak clearly appears in the shaded region due to constructive interference of the quadrupole plasmons in the metamaterial lattice.
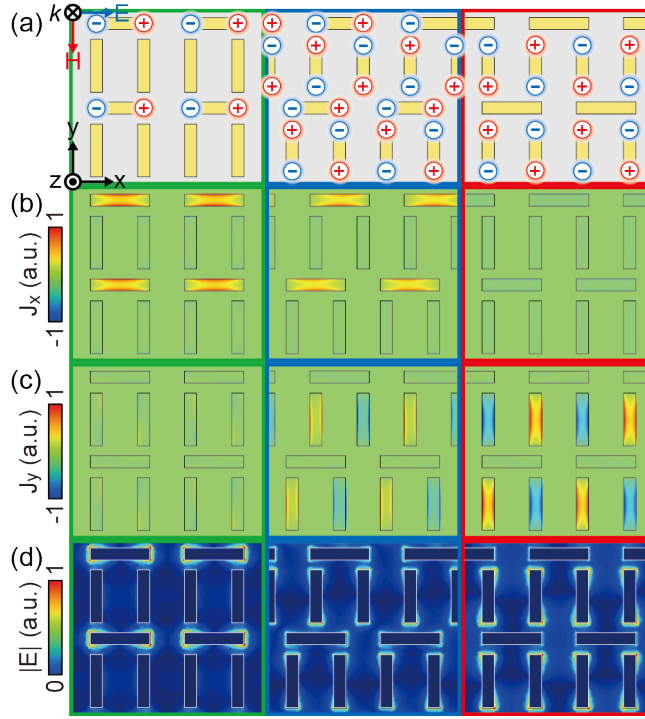
FIG 3. Mode profiles of metamaterials. (a) Schematic of the charge distributions and numerically simulated (b) J_x, (c) J_y, and (d) |E| distributions at 1750 cm^{-1} in Fig. 2(b). For d = 0 (the left column), only the dipole mode in the Au bars is allowed due to the near-field coupling between the vertical neighboring unit cells, while the quadrupole mode in the Au bar pairs is constructively excited for $d = P_x/2$ (the right column). The $d = P_x/4$ (the center column) is the intermediate state where both the dipole and quadrupole modes are excited simultaneously.
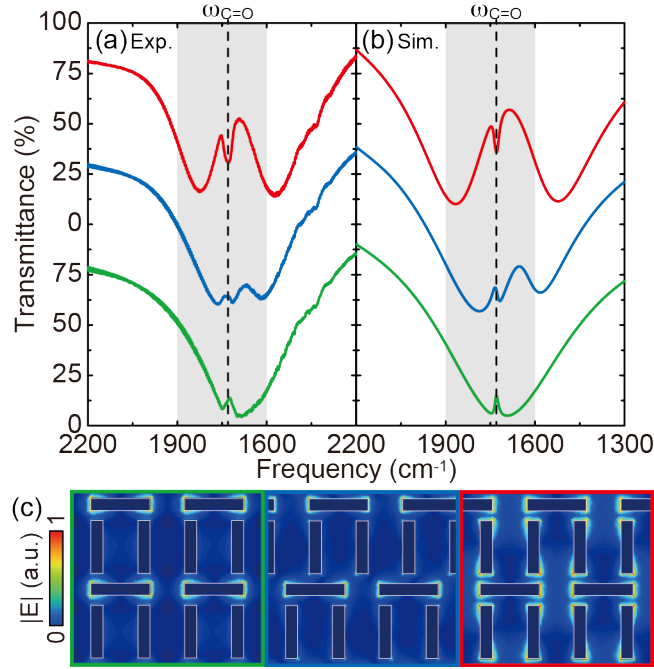
FIG 4. EIT metamaterial-enhanced IR absorption. (a) Experimentally measured transmission spectra of a 50-nm thick PMMA film on the metamaterials and (b) corresponding numerical simulations. The resonant coupling of the quadrupole (dipole) and C=O modes at $\omega_{C=O}$, indicated by the dashed lines, results in an anti-resonant dip (peak) within the spectral line-shape of the metamaterials. (c) Numerically simulated $|E|$ distributions at $\omega_{C=O}$ in (b). The highly-dispersive dense quadrupole mode for $d = P_x/2$ (the right) is strongly disturbed by the C=O mode, giving a stronger molecular signal compared to the dipole mode case for $d = 0$ (the left).